Journal of Power Sources 196 (2011) 6670–6675

Contents lists available at ScienceDirect

Journal of Power Sources

journal homepage: www.elsevier.com/locate/jpowsour

Preparation of hierarchical porous carbon and its rate performance as anode of lithium ion battery

J. Yi [a], X.P. Li [a,b,c], S.J. Hu [a,b,c], W.S. Li [a,b,c,*], L. Zhou [a], M.Q. Xu [a,b,c], J.F. Lei [a], L.S. Hao [a]

[a] School of Chemistry and Environment, South China Normal University, Guangzhou 510006, China
[b] Key Laboratory of Electrochemical Technology on Energy Storage and Power Generation of Guangdong Higher Education Institutes, South China Normal University, Guangzhou 510006, China
[c] Engineering Research Center of Materials and Technology for Electrochemical Energy Storage (Ministry of Education), South China Normal University, Guangzhou 510006, China

ARTICLE INFO

Article history:
Received 20 July 2010
Received in revised form 2 December 2010
Accepted 8 December 2010
Available online 21 December 2010

Keywords:
Hierarchical porous carbon
Anode
Rate performance
Lithium ion battery

ABSTRACT

A hierarchical porous carbon with low oxygen content has been prepared by using polystyrene (PS) spheres as template and its structure, composition and performances as anode of lithium ion battery are characterized by scanning electron microscopy (SEM), transmission electron microscopy (TEM), X-ray diffraction (XRD), Fourier transform infrared (FTIR) spectroscopy, element analysis (EA), electrochemical impedance spectroscopy (EIS), and galvanostatic charge/discharge test. The results obtained from SEM, TEM, XRD, FTIR, and EA indicate that the prepared sample has a well-interconnected pore structure with a pore size of 170 nm and has an oxygen content of 3.3 ± 0.2 wt.%. The low oxygen content of the prepared sample can be ascribed to the low decomposition temperature of the template that was determined by thermal analysis. EIS shows that the prepared sample has lower electrochemical impedance for the lithium insertion/de-insertion than commercial natural graphite and charge/discharge tests show that the battery using the prepared sample as anode exhibits better rate performance than that using the graphite.

1. Introduction

To meet the demand for the reduction of carbon emission, electric vehicles (EVs) need to be developed. The successful application of EVs depends to a great extent on the power and energy densities of power sources. Lithium ion battery (LIB) is believed to be the best power source for EVs in near further, because it has the largest energy density among all the commercial secondary batteries [1–8]. Present commercial lithium ion batteries use graphite as anode materials, which have many advantages including cheap cost and eco-friendliness. However, the poor rate performance of LIBs using graphite materials yields low power density. Therefore, many researches are focused on the development of new carbon materials that have fast kinetics of lithium ion insertion/de-insertion [9–12]. Among these carbon materials, hierarchical porous carbon is effective for the improvement in kinetics of lithium ion insertion/de-insertion because it provides large surface as well as uniform pore structure. The hierarchical pores provide carbon with large surface for the electron transfer reaction and short way for lithium ion diffusion in carbon matrix, which are the main factors that determine the rate performance of lithium ion batteries [11,12].

Different hierarchical porous carbon materials have been synthesized by using inorganic or polymer templates, such as aluminophosphate [13], aluminosilicate [14], poly(methylmethacrylate) (PMMA) [15]. In the synthesis of hierarchical porous carbon by using inorganic templates, the preparation and the removal of inorganic templates are complex. For example, the preparation of silica templates needs calcination and their removal needs etching by NaOH. Comparatively, the application of polymer templates is simple. The preparation and the removal of polymer templates proceed usually under mild conditions. Most importantly, the polymer templates can serve as the part of carbon sources in the buildup of the hierarchical porous carbon. However, the hierarchical porous carbon prepared by using polymer templates contains large amount of oxygen, which increases the irreversible capacity loss of carbon electrodes in lithium ion battery due to the formation of inactive lithium oxide [15–18]. It has been reported that monolithic macroporous carbon prepared using close-packed PMMA spheres as template has an oxygen content of 8.0 ± 0.6 wt.% [15].

In this paper, we proposed a new method for the preparation of hierarchical porous carbon by using polystyrene (PS) spheres as template. The prepared sample has low oxygen content and

* Corresponding author at: School of Chemistry and Environment, South China Normal University, Guangzhou 510006, China.
Tel.: +86 20 39310256; fax: +86 20 39310256.
E-mail address: liwsh@scnu.edu.cn (W.S. Li).

0378-7753/$ – see front matter © 2010 Elsevier B.V. All rights reserved.
doi:10.1016/j.jpowsour.2010.12.017

exhibits excellent rate and cycle performance when used as anode of lithium ion battery.

2. Experimental

2.1. Preparation of hierarchical porous carbon

Noncross-linked and monodisperse PS spheres were synthesized according to the reported procedure [19]. The corresponding reaction is:

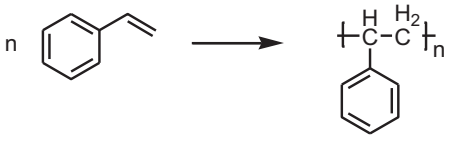

(1)

Styrene was purified with 0.1 M NaOH three times and then with deionised water three times. The purified styrene (26 mL) and 1.25 wt.% sodium persulfate solution (40 mL) were added successively into a mixed solution of 200 mL deionised water and 1.8 g polyvinylpyrrolidone (PVP) at 70 °C and under stirring in N_2 atmosphere. The reaction proceeded at 70 °C for 24 h and PS spheres were obtained by centrifugalizing the resulting mixture.

Porous carbon was prepared as follows: 12 mmol resorcinol and 24 mmol formaldehyde were mixed with 1.92 mL water, 0.06 mmol sodium carbonate (as catalyst) and 2 g PS spheres at room temperature under gentle stirring for 30 min. Then the PS spheres were separated from the mixture by filtration and dried at 85 °C in vacuum for three days, resulting in a close-packed structure with its space full of resorcinol-formaldehyde (RF) gel. The resulting gel was carbonized at 900 °C for 2 h under an Ar atmosphere. The involved reactions are:

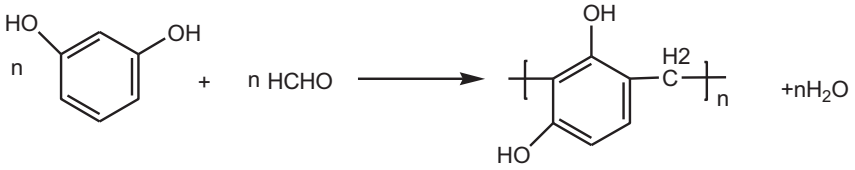

(2)

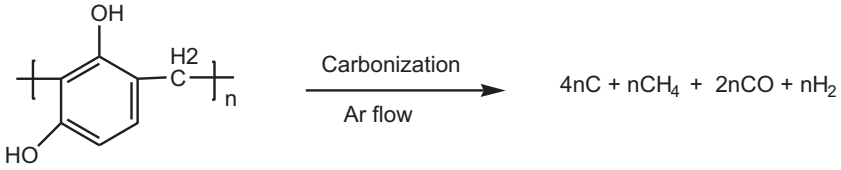

(3)

All the chemicals were purchased from Sinopharm Chemical Reagent Co., Ltd. and used without further purification except for styrene.

2.2. Characterization

The crystal structure of the prepared sample was characterized by X-ray diffraction (XRD, Rigaku D/MAX-RC, Japan) with CuKα radiation (k = 1.54178 Å) at 30.0 kV and 20 mA. The scattering angle range used in the measurements was from 10° to 70°. The morphology of the prepared sample was observed with scanning electron microscopy (SEM, JEOL, JSM-6380LV, Japan) and transmission electron microscopy (TEM, JEOL, JEM-2010HR, Japan). Elemental contents of the sample were analyzed on VarioEL III (Germany). Fourier transform infrared (FTIR) spectra was obtained with a PerkinElmer instrument (USA) using KBr pellet technique. Thermal analysis (TG–DSC) was carried out on NETZSCH STA 409C thermal analyzer (Germany), in which the sample was heated in alumina crucible under N_2 flow to 900 °C at 4 °C min^{-1}. The N_2-sorption isotherm curve was recorded at 77 K on Micromeritics ASAP 2020 instrument (USA). Specific surface areas were calculated by the Brunauer–Emmett–Teller (BET) method, pore sizes and volumes were estimated from pore size distribution from the desorption branch of the isotherm.

2.3. Electrode preparation and performance determination

80 wt.% prepared carbon sample as active material, 10 wt.% acetylene black as conducting agent and 10 wt.% polyvinylidene fluoride (PVDF) as binder were mixed using N-methylpyrrolidone (NMP) as solvent. Electrode film was prepared by coating the mixture on copper foil and dried successively in air at 85 °C for 2 h and in a vacuum oven at 130 °C for 4 h. For a comparison, commercial natural graphite with the average diameter of 27 μm (Superior Graphite Company) was also used as active material to prepare electrode film under the same conditions. The unit weights of active materials in both electrode films were about 7 ± 0.2 mg cm^{-2}.

Electrochemical measurements were carried out by using a coin-type test cell (CR2032), where carbon sample was used as anode, Li metal foil was used as cathode, 1 M $LiPF_6$ in EC:DMC:EMC (1:1:1 in volume) was used as electrolyte, and Celgard 2400 membrane was used as separator. The assembly of the cell was conducted in an Ar-filled glove box (Mikrouna, Super 1220/750/900). The assembled cells were aged overnight before test. Electrochemical impedance spectroscopic (EIS) measurements were conducted on PGSTAT 30 (Autolab) controlled by FRA software, the frequencies were from 10 mHz to 100 kHz with an amplitude of 5 mV. Galvanostatic charge/discharge tests were performed on Land CT 2001A (China) with different current densities at the potentials between 0.01 and 2 V (vs. Li^+/Li).

3. Results and discussion

Fig. 1 presents the SEM and TEM images of the prepared carbon sample. The SEM image (Fig. 1a) shows a porous structure with the pore size of about 170 nm in diameter and small holes of 20–30 nm on the pore. The TEM image (Fig. 1b) shows the different brightness of circles and their overlapped shape. The circles have the same diameter as the pore of 170 nm observed by SEM, confirming that spherical pores in the sample were successfully formed. The different brightness of the circles indicates that the pores in the sample are in different layers and the overlapped shapes indicate that the pores are interconnected with neighboring pores, which forms the small holes of 20–30 nm. Therefore, the prepared sample is a hierarchical porous carbon, which has ordered and interconnected pore structure.

Element analysis was carried out to determine the composition of the prepared carbon sample. The obtained results are (in wt.%): C (87.3 ± 0.1), H (1.1 ± 0.1), N (1.4 ± 0.1), O (3.3 ± 0.2), S

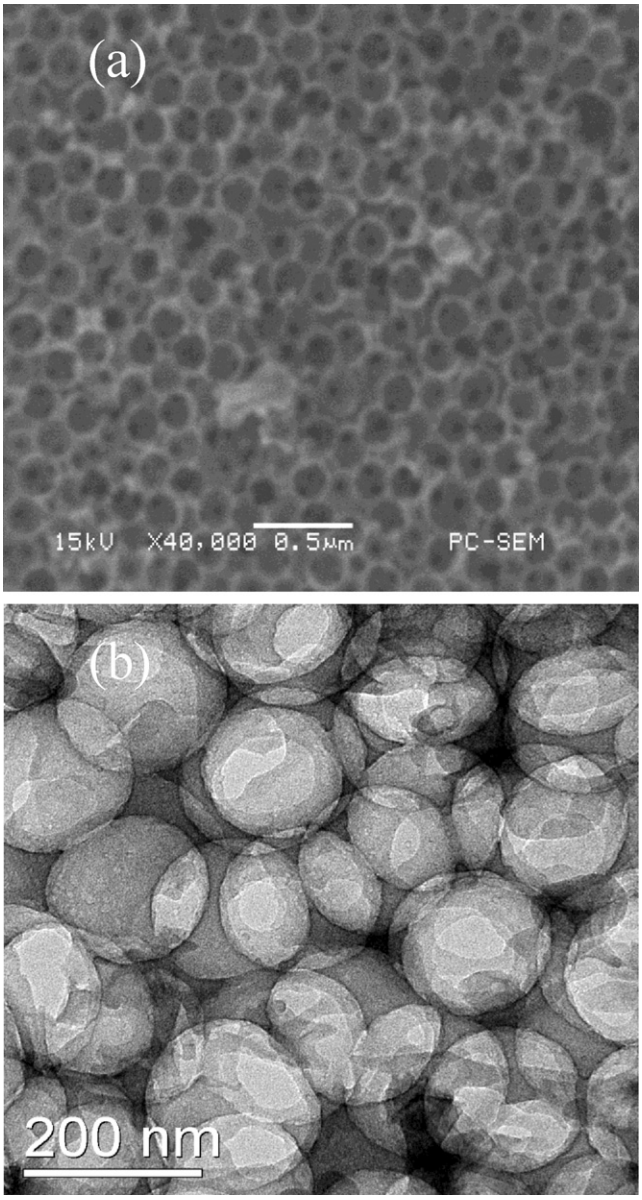

Fig. 1. SEM (a) and TEM (b) images of the prepared carbon sample.

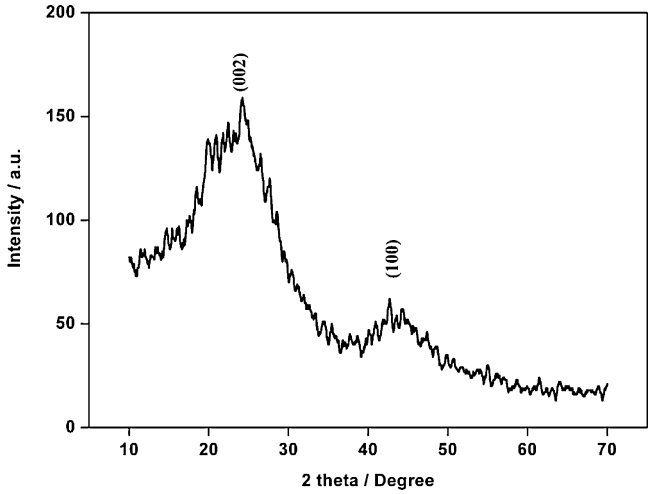

Fig. 2. XRD patterns of the prepared hierarchical porous carbon.

(0.7 ± 0.1). It can be known from the element analysis that the prepared sample consists mainly of carbon with small amount of oxygen, nitrogen, hydrogen, and sulfur. The sulfur might be the residues from sodium persulfate used in polymerization preparation of PS sphere and the nitrogen might be from the adsorption of N_2 in air during the sample transfer. The estimated oxygen content in the hierarchical porous carbon is 3.3 ± 0.2 wt.%, which is much lower than that in other porous carbon materials [20]. Porous carbon materials contain usually large amount of oxygen, which comes from the precursor of carbon sources. For example, the carbon synthesized by using RF resin as carbon source contains an oxygen content of 6.84 wt.% [20]. Especially, the hierarchical porous carbon synthesized by using RF resin as carbon source and using PMMA as template contains an oxygen content of 8.0 ± 0.6 wt.% [15]. Such a large oxygen content can be ascribed to the use of PMMA ($(C_5O_2H_8)_n$) template that contains oxygen and has a high decomposition temperature. The template as the pore former of porous carbon sample functions also as carbon source and its high decomposition temperature affects the escaping of the oxygen in itself and the precursor. The higher decomposition temperature will block the escaping of oxygen, resulting in the higher oxygen content in the carbon sample. In this work, we used PS as template, which does not contain any oxygen and has lower decomposition temperature. Thus, we provide a method for the hierarchical porous carbon with low content of oxygen. It has been reported that the higher oxygen content in carbon samples yields a larger irreversible capacity loss as anode of lithium ion battery due to the formation of inactive lithium oxide [16,17]. Furthermore, it can be understood that the inactive lithium oxide will impede the charge transfer process of the lithium insertion/de-insertion reaction and thus reduce the rate performance of the sample. Therefore, it can be expected that our hierarchical porous carbon has better rate performance as anode of lithium ion battery.

Fig. 2 presents the XRD pattern of the prepared hierarchical porous carbon. It can be seen from Fig. 2 that there are two broad diffraction peaks at ca 22° and 44°, corresponding to the (0 0 2) and (1 0 0) reflections of carbon, respectively, which suggests that the sample is predominantly made up of single-layer carbon sheets that are not stacked in a parallel fashion. Therefore, there must be small pores or voids between the carbon sheets [15,21].

Fig. 3 presents the FTIR spectra of the precursor (PS spheres with RF resin) and the prepared hierarchical porous carbon. As shown in Fig. 3a, the absorption peak at 3228 cm^{-1} of the precursor corresponds to the stretching vibration of O–H, which can be ascribed to the hydroxyl group in resorcinol. Four characteristic peaks of the phenyl ring in PS template can be found from 1600 to 1450 cm^{-1}. Sharp peaks at 3021 cm^{-1} and 754, 695 cm^{-1} correspond to the stretching vibration and bending vibration of C–H in the phenyl ring. The $-CH_2-$ bending vibration in PS can be found at the peaks around 1470 cm^{-1}. The absorption band at 1603 cm^{-1} is assigned to the stretching vibrations of aromatic ring. The peaks at 1093 cm^{-1} and 1220 cm^{-1} associated with C–O–C stretching vibrations of methylene ether bridges between resorcinol molecules [22,23]. Thus PS and RF resin exist in the precursor [24].

In the hierarchical porous carbon, as shown in Fig. 3b, there are the bending vibrations of ester group at 1192 cm^{-1} in phenolic materials, aliphatic C–H at 1380 cm^{-1}, and aromatic –CH at 1593 cm^{-1}, but the typical peaks of PS cannot be observed. This indicates that there is some residue of RF resin but all the PS is pyrolyzed. The absorption peak at 3421 cm^{-1} corresponds to the stretching vibration of O–H in water molecules [25]. The water may be adsorbed on the sample during transferring sample in the air for the FTIR determination.

The conversion of PS and RF into carbon can be observed from the weight losses of the precursor upon pyrolysis, as shown in Fig. 4.

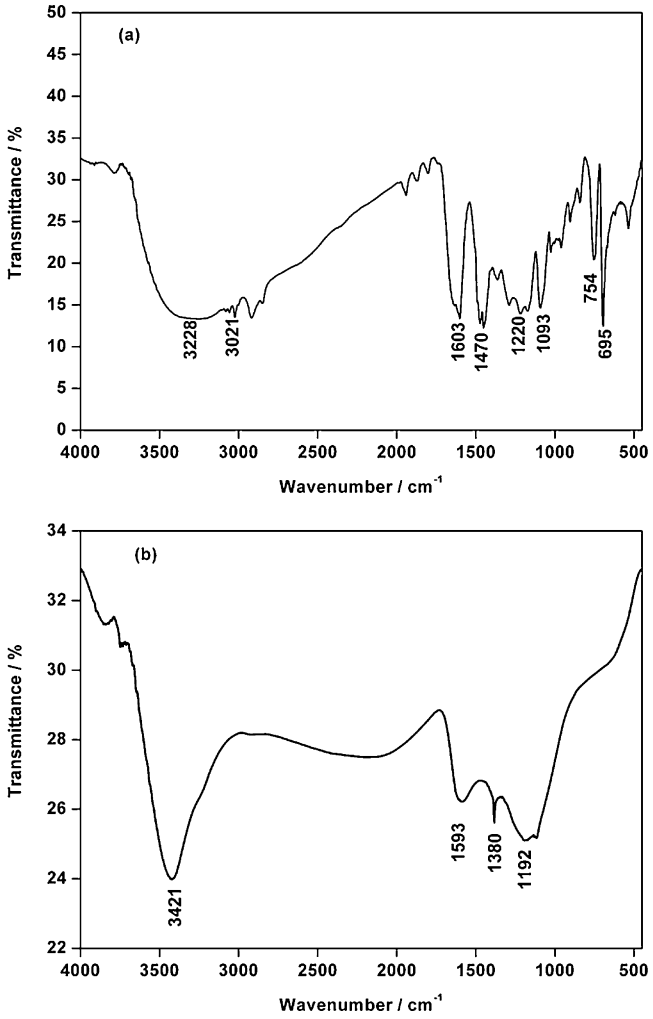

Fig. 3. FTIR spectra of the precursor (resorcinol-formaldehyde resin and polystyrene spheres) (a) and the hierarchical porous carbon (b).

There is a loss of about 80% mass when the pyrolysis temperature is higher than 800 °C. Three major weight losses of different extent in the temperature range of 25–900 °C can be observed. The first weight loss at 25–375 °C is mainly due to the desorption of physisorbed water and evolution of byproducts from cross-linking

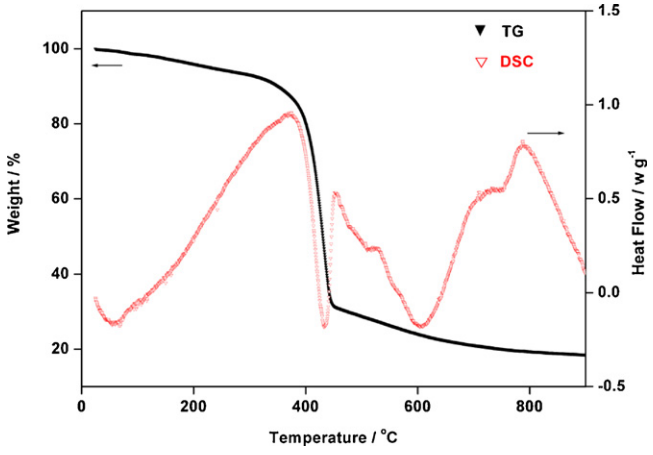

Fig. 4. TG/DSC curves of the precursor (resorcinol-formaldehyde resin and polystyrene spheres) for the synthesis of hierarchical porous carbon. The arrows show the corresponding coordinate axes of the curves.

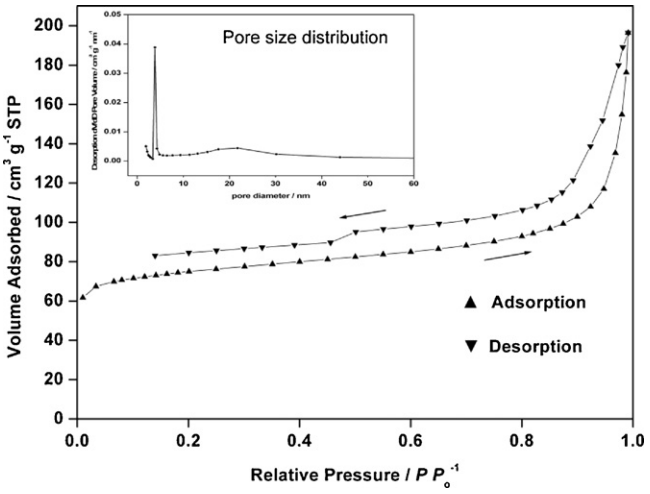

Fig. 5. Nitrogen adsorption isotherm and BJH pore size distribution (inset) for the hierarchical porous carbon. The arrows show the change directions of pressure.

reactions of RF resin preparation, showing the endothermic peak at 65 °C and the exothermic peak at 375 °C in DSC curve. The second weight loss at 375–450 °C can be attributed to the decomposition of PS, which is accompanied by a large endothermic peak of at 440 °C in DSC curve [26], which indicates that the decomposition temperature of PS is lower than 450 °C. The third weight loss at 450–900 °C can be attributed to the decomposition of RF resin and the formation of gas CH_4, H_2, and CO, corresponding to the endothermic peak of at 600 °C and exothermic peak of at 800 °C in DSC curve [20], which suggests that the decomposition of RF resin involves a slow reaction process and confirms the residue of the RF observed in Fig. 3b. It is clear that PS can be converted into carbon more easily than the RF resin and the PMMA whose decomposition temperature is 625 °C [27]. The lower decomposition temperature of template favors the escaping of the oxygen in RF, because the RF is covered by the template. The effect of the template explains why the hierarchical porous carbon prepared by using PS as template has lower oxygen content than those prepared by using other templates. Therefore, PS is a good template for the preparation of hierarchical porous carbon with low oxygen content.

Fig. 5 presents the adsorption/desorption isotherm of the hierarchical porous carbon along with its pore size distribution derived from the desorption branch of the isotherm. The adsorption belongs to a type-II isotherm that is characteristic of macroporous solid materials. This is consistent with the pore size (170 nm) of the hierarchical porous carbon. From the BJH curve, it can be seen that there are two kinds of mesopores in the hierarchical porous carbon, 3 nm and 20 nm in average, respectively. The mesopores of 3 nm can be ascribed to the randomly arranged carbon sheets that are not stacked in parallel, as indicated in XRD pattern of Fig. 2. While the mesopores of 20 nm can be ascribed to the holes (20–30 nm) resulted from the overlapping of the neighboring pores in the hierarchical porous carbon, as shown in Fig. 1. The surface area that the mesopores contribute to, determined from the βs plot, is about 62 $m^2 g^{-1}$ [28,29]. However, the Brunauer–Emmett–Teller (BET) specific surface area, calculated from the N_2-adsorption data, is 254 $m^2 g^{-1}$. Therefore, the specific surface area of the hierarchical porous carbon mainly results from its macropores (170 nm) that are formed by PS spheres.

Fig. 6 presents the charge/discharge profiles of the hierarchical porous carbon at a current density of 18.6 mA g^{-1}, with a comparison of commercial natural graphite. In the first cycle, the charge and discharge capacity is 716 and 277.9 mAh g^{-1} for the hierarchical

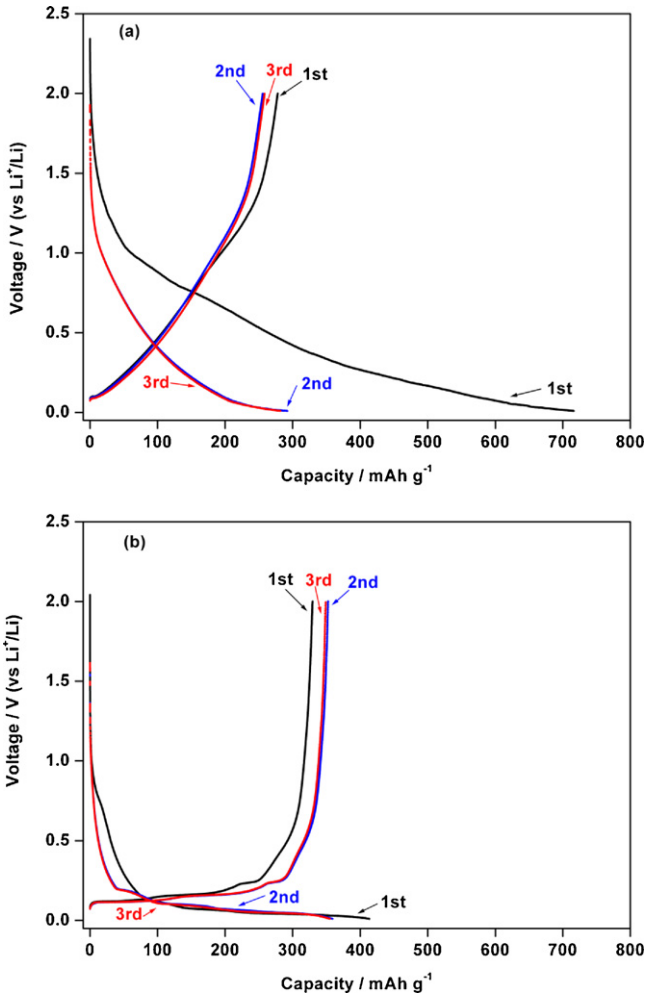

Fig. 6. Charge/discharge profiles of the hierarchical porous carbon (a) and the commercial natural graphite (b) at a current density of 18.6 mA g^{-1}.

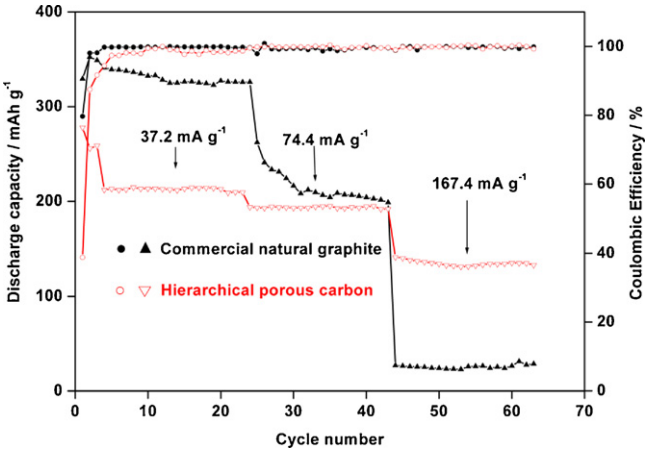

Fig. 7. Cyclic performance of hierarchical porous carbon and the commercial natural graphite at different charge/discharge current densities.

porous carbon, while 413.4 and 329.5 mAh g^{-1} for the commercial natural graphite, respectively. The hierarchical porous carbon shows a larger irreversible capacity loss than the commercial natural graphite, as reported by other researchers [16,17,20]. The hierarchical porous carbon has a large surface area due to its porous structure, which needs a large amount of electrical quantity to form the solid state interphase during charge, and the existence of oxygen needs electrical quantity for the formation of the inactive lithium oxdie, resulting in the larger irreversible capacity loss of the hierarchical porous carbon than the commercial natural graphite.

Fig. 7 presents the rate and cycle performance of the hierarchical porous carbon in comparison with the commercial natural graphite. The specific currents used were 18.6 mA g^{-1}, 37.2 mA g^{-1}, 74.4 mA g^{-1}, and 167.4 mA g^{-1}. The specific current densities were based on the same mass for the electrode preparation. When a specific current of 18.6 mA g^{-1} is applied to the hierarchical porous carbon electrode, a specific discharge capacity of 277.9 mAh g^{-1} is obtained. The specific capacity decreases with increasing the charge/discharge current. At 167.4 mA g^{-1}, the specific capacity decreases to 50% of the capacity at 18.6 mA g^{-1}. Compared with the commercial natural graphite, the hierarchical porous carbon shows a better rate performance. It can be noted that the capacity loss of the hierarchical porous carbon can be neglected when cycling at different rates. For example, the capacity is 193.7 mAh g^{-1} for the first cycle and remains 191.9 mAh g^{-1} after 20 cycles at 74.4 mA g^{-1}, as shown in Fig. 8a. Additionally, after 20 cycles at each rate the capacity of the hierarchical porous carbon can be restored to about 273 mAh g^{-1} at 18.6 mA g^{-1} (data not shown). This indicates that the hierarchical porous carbon also has good cycle performance. The large surface area and low oxygen content of the hierarchical porous carbon contribute to its good rate performance and its good structure with the pores distributing uniformly contributes to its good cycle performance.

The interconnected pores of the hierarchical porous carbon provide fast paths for lithium ion transportation in materials and large surface for the charge transfer of lithium insertion/de-insertion reaction, which are the important factors for rate performance. The fast kinetics of lithium ion insertion/de-insertion can be confirmed by the results obtained from electrochemical impedance measurements. Fig. 8 presents the Nyquist plots of the cells at open-circuit voltage and the equivalent circuit representing the lithium ion insertion/de-insertion process. In the equivalent circuit, *Rs* is the ohmic resistance of the electrolyte and the current collector, Q_1 is the surface film capacitance (C_f), R_f is the resistance for Li^+ migration through the surface film, Q_2 is the double-layer capacitance (C_{dl}), R_{ct} is the charge-transfer resistance at the bulk-electrolyte interface. Z_W is related to Li^+ diffusion in the inserted materials, and C_{int} is related to insertion capacitance reflecting the occupation of Li^+ into the inserted sites [30–32]. It can be seen from Fig. 8 that the experimental data (dots) can be well fitted by the equivalent circuit

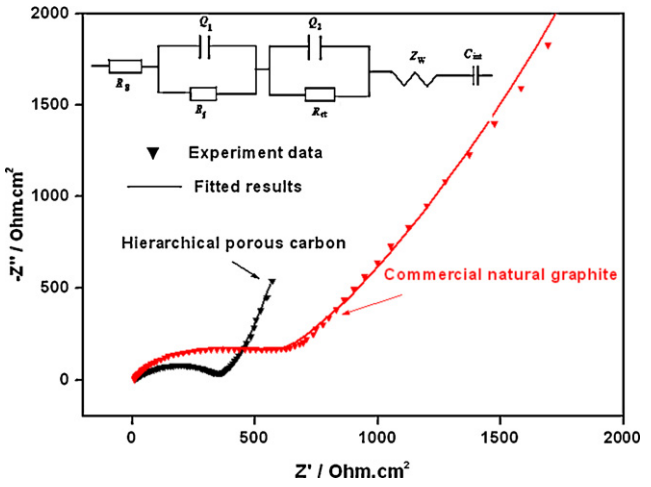

Fig. 8. Nyquist plots of the hierarchical porous carbon and the commercial natural graphite electrodes at open-circuit voltage.

(the solid lines represent the fitted results). The resistance ($R_{ct} + R_f$) obtained from fitting by the equivalent circuit, which determines the charge transfer process of lithium ion insertion/de-insertion reaction, is 346 and 546 Ω for the hierarchical porous carbon and the commercial nature graphite, respectively. The lower resistance ($R_{ct} + R_f$) confirms that the hierarchical porous carbon has a faster charge transfer process. As shown in Fig. 8, the hierarchical porous carbon has far lower diffusion impedance (Z_w) than the commercial natural graphite, which is certainly ascribed to the porous structure of the hierarchical porous carbon. The pore-interconnected framework of the hierarchical porous carbon provides the paths for the easy accessibility of electrolytes and the fast diffusion of lithium ions. The faster charge transfer process of lithium insertion/de-insertion reaction and the faster diffusion of lithium ions contribute to the better rate performance of the hierarchical porous carbon than the commercial natural graphite as anode of lithium ion battery.

4. Conclusions

We reported a new method for the preparation of hierarchical porous carbon with low oxygen content. With polystyrene spheres used as template for the pore formation, the prepared hierarchical carbon with low oxygen content can be obtained because polystyrene does not contain any oxygen and has low decomposition temperature. The prepared hierarchical porous carbon has low electrochemical impedance for lithium insertion/de-insertion and thus exhibits better rate performances than commercial natural graphite as anode material for lithium ion battery.

Acknowledgements

This work is supported by the National Natural Science Foundation of China (grant no. NSFC20873046), Specialized Research Fund for the Doctoral Program of Higher Education (grant no. 200805740004) and Natural Science Foundation of Guangdong Province (grant no. 10351063101000001).

References

[1] L.D. Xing, C.Y. Wang, W.S. Li, M.Q. Xu, X.L. Meng, S.F. Zhao, J. Phy. Chem. B 113 (2009) 5181.
[2] L.D. Xing, W.S. Li, C.Y. Wang, F.L. Gu, M.Q. Xu, C.L. Tan, J. Yi, J. Phys. Chem. B 113 (2009) 16596.
[3] C.L. Tan, H.J. Zhou, W.S. Li, X.H. Hou, D.S. Lu, M.Q. Xu, Q.M. Huang, J. Power Sources 184 (2008) 408.
[4] M.Q. Xu, L.D. Xing, W.S. Li, X.X. Zuo, D. Shu, G.L. Li, J. Power Sources 184 (2008) 427.
[5] T. Jiang, S.C. Zhang, X.P. Qiu, W.T. Zhu, L.Q. Chen, J. Power Sources 166 (2007) 503.
[6] X.F. Zhang, J. Liu, H.Y. Yu, G.L. Yang, J.W. Wang, Z.J. Yu, H.M. Xie, R.S. Wang, Electrochim. Acta 55 (2010) 2414.
[7] M.Q. Xu, W.S. Li, X.X. Zuo, J.S. Liu, X. Xu, J. Power Sources 174 (2007) 705.
[8] W.J. Cui, H.J. Liu, C.X. Wang, Y.Y. Xia, Electrochem. Commun. 10 (2008) 1587.
[9] J.C. Chang, Y.F. Tzeng, J.M. Chen, H.T. Chiu, C.Y. Lee, Electrochim. Acta 54 (2009) 7066.
[10] S. Flandrois, B. Simon, Carbon 37 (1999) 165.
[11] F. Zhang, K.X. Wang, G.D. Li, J.S. Chen, Electrochem. Commun. 11 (2009) 130.
[12] W. Xing, P. Bai, Z.F. Li, R.J. Yu, Z.F. Yan, G.Q. Luc, L.M. Lu, Electrochim. Acta 51 (2006) 4626.
[13] G. Liu, Y. Liu, Z.L. Wang, X.Z. Liao, S.J. Wu, W.X. Zhang, M.J. Jia, Micropor. Mesopor. Mater. 116 (2008) 439.
[14] J. Lee, K. Sohn, T. Hyeon, J. Am. Chem. Soc. 123 (2001) 5146.
[15] K.T. Lee, J.C. Lytle, N.S. Ergang, S.M. Oh, A. Stein, Adv. Funct. Mater. 15 (2005) 547.
[16] W.M. Lu, D.D.L. Chung, Carbon 39 (2001) 493.
[17] A.M. Wilson, W. Xing, G. Zank, B. Yatesd, J.R. Dahn, Solid State Ionics 100 (1997) 259.
[18] W. Xing, A.M. Wilson, G. Zank, J.R. Dahn, J. Electrochem. Soc. 144 (1997) 2410.
[19] T. Sen, G.J.T. Tiddy, J.L. Casci, M.W. Anderson, Angew. Chem. Int. Ed. 42 (2003) 4649.
[20] M. Yoshimune, T. Yamamoto, M. Nakaiwa, K. Haraya, Carbon 46 (2008) 1031.
[21] T. Zheng, Q. Zhong, J.R. Dahn, J. Electrochem. Soc. 142 (1995) L211.
[22] R.W. Pekala, J. Mater. Sci. 24 (1989) 3221.
[23] L. Zhang, H.B. Liu, M. Wang, L. Chen, Carbon 45 (2007) 1439.
[24] L.J. Fu, T. Zhang, Q. Cao, H.P. Zhang, Y.P. Wu, Electrochem. Commun. 9 (2007) 2140.
[25] N. Kishore, S. Sachan, K.N. Rai, A. Kumar, Carbon 41 (2003) 2961.
[26] R.W.J. Westerhout, J. Waanders, J.A.M. Kuipers, W.P.M. Van Swaaij, Ind. Eng. Chem. Res. 36 (1997) 1955.
[27] M. Ferriola, A. Gentilhommea, M. Cocheza, N. Ogetb, J.L. Mieloszynski, Polym. Degrad. Stab. 79 (2003) 271.
[28] W.W. Lukens, G.D. Stucky, Chem. Mater. 14 (2002) 1665.
[29] W.W. Lukens, P. Schmidt-Winkel, D.Y. Zhao, J.L. Feng, G.D. Stucky, Langmuir 15 (1999) 5403.
[30] M.D. Levi, D. Aurbach, J. Phys. Chem. B 101 (1997) 4630.
[31] M.D. Levi, D. Aurbach, J. Phys. Chem. B 101 (1997) 4641.
[32] D.S. Lu, W.S. Li, X.X. Zuo, Z.Z. Yuan, Q.M. Huang, J. Phy. Chem. C 111 (2007) 12067.